





## Article

# Conversion of Xylose to Furfural over Lignin-Based Activated Carbon-Supported Iron Catalysts

Annu Rusanen <sup>1,\*</sup>, Riikka Kupila <sup>2</sup>, Katja Lappalainen <sup>1,2</sup>, Johanna Kärkkäinen <sup>1</sup>, Tao Hu <sup>1</sup>  
and Ulla Lassi <sup>1,2</sup>

<sup>1</sup> Research Unit of Sustainable Chemistry, University of Oulu, P.O. Box 4300, FIN-90014 Oulu, Finland; katja.lappalainen@oulu.fi (K.L.); johanna.karkkainen@oulu.fi (J.K.); tao.hu@oulu.fi (T.H.); ulla.lassi@oulu.fi (U.L.)

<sup>2</sup> Unit of Applied Chemistry, Kokkola University Consortium Chydenius, University of Jyväskylä, FI-67100 Kokkola, Finland; riikka.kupila@chydenius.fi

\* Correspondence: annu.rusanen@oulu.fi; Tel.: +358-294-48-1636

Received: 30 June 2020; Accepted: 20 July 2020; Published: 22 July 2020



**Abstract:** In this study, conversion of xylose to furfural was studied using lignin-based activated carbon-supported iron catalysts. First, three activated carbon supports were prepared from hydrolysis lignin with different activation methods. The supports were modified with different metal precursors and metal concentrations into five iron catalysts. The prepared catalysts were studied in furfural production from xylose using different reaction temperatures and times. The best results were achieved with a 4 wt% iron-containing catalyst, 5Fe-ACs, which produced a 57% furfural yield, 92% xylose conversion and 65% reaction selectivity at 170 °C in 3 h. The amount of Fe in 5Fe-ACs was only 3.6  $\mu\text{mol}$  and using this amount of homogeneous  $\text{FeCl}_3$  as a catalyst, reduced the furfural yield, xylose conversion and selectivity. Good catalytic activity of 5Fe-ACs could be associated with iron oxide and hydroxyl groups on the catalyst surface. Based on the recycling experiments, the prepared catalyst needs some improvements to increase its stability but it is a feasible alternative to homogeneous  $\text{FeCl}_3$ .

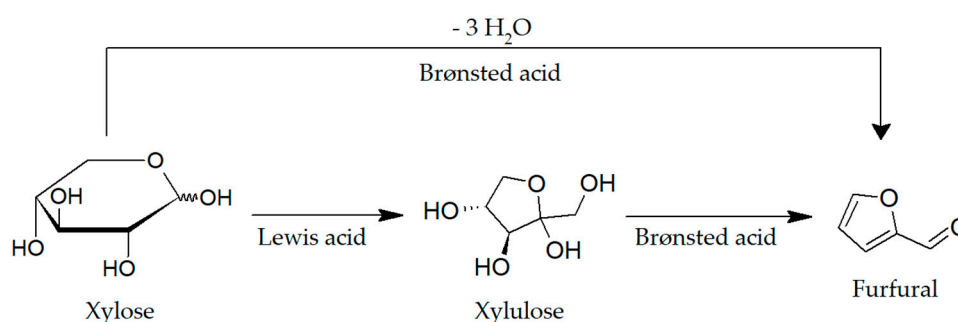
**Keywords:** furfural; carbon-supported catalyst; xylose conversion; iron; heterogeneous catalysts

## 1. Introduction

Furfural is an important biomass-based high-value chemical with numerous applications [1]. While it is widely used directly as a solvent and a fungicide, it is most commonly converted into pharmaceuticals, chemicals and biopolymers, many of which are used as substitutes for petrochemical-derived analogs [2,3].

Approximately 300,000 tons of furfural are produced annually and the biggest manufacturer is China [4]. It is formed by the dehydration of pentoses, mainly xylose, which can be obtained through the hydrolysis of different agricultural residues (corn stover, wheat straw, sugarcane bagasse, rice husk, oat hull) or forest industry wastes (birch or poplar sawdust). Current industrial processes use mineral acids, such as sulfuric, phosphoric or hydrochloric acid, as catalysts, with an approximate furfural yield of 50% [5,6]. The relatively low yield, high energy consumption (caused by the high, 150–240 °C, reaction temperature) and environmental concerns related to acidic process wastes are driving scientists to develop catalysts with high selectivity for furfural formation. A number of studies have used inexpensive water-soluble inorganic salts (mainly chlorides) as catalysts instead of mineral acids for xylose conversion to furfural [7–10]. Many of those studies show that  $\text{FeCl}_3$  results in the highest furfural yields compared to other metal chlorides [7,10].

Compared to water-soluble salts, solid catalytic systems have fewer environmental impacts than liquid ones, reduce operational costs and are technically feasible alternatives for industry [11]. A broad range of different heterogeneous catalysts have been studied for xylose conversion to furfural, the most common of which are acidic zeolites and mesoporous silicas, such as SBA-15 and MCM-41 [11,12]. Additionally, sulfonated metal oxides (especially  $\text{TiO}_2$ ,  $\text{ZrO}_2$ ) have been used, either as such or combined with mesoporous supports [13–16]. Many studies have shown that some Brønsted acidity is needed, either from metal oxide or support, in addition to metal oxides with a Lewis character, to achieve good furfural yields [17,18]. The need for Brønsted acidity is associated with the furfural production mechanism; while Lewis acid can isomerize xylose to xylulose, Brønsted acid is needed for the dehydration step (Scheme 1) [19].



**Scheme 1.** Dehydration of xylose to furfural by Brønsted acid and Lewis acid catalysts.

Carbon-based catalysts are attractive since the carbon supports are low-cost materials with high surface area and good thermal stability and they are easily modified with functional groups [20]. Carbon surface groups containing heteroatoms, such as oxygen, can act as anchoring sites for metal particles and generate high metal dispersion [21]. The diverse surface also enables Brønsted acidity in addition to metal's Lewis acidity, which can further promote xylose conversion to furfural. To the best of our knowledge, few papers have been published on carbon-supported metal oxide catalysts. Mazzotta et al. used a sulfonated carbonaceous material with  $\text{TiO}_2$  sites, while Russo et al. used  $\text{TiO}_2$ /carbon black in the conversion of xylose to furfural [22,23]. Barroso-Bogeat et al. prepared a class of different activated carbon-metal oxide catalysts (Fe, Al, Zn, Sn, Ti and W) but did not use them in any reaction [24–26]. Therefore, cheap metal oxides, such as iron oxide, have not been utilized in xylose conversion to furfural, even though iron is common in homogeneous catalysts. The aim of this study was to create iron oxide sites on a carbon-supported catalyst and apply the catalyst in the conversion of xylose to furfural. Activated carbon support was derived from hydrolysis lignin, which is a side stream of cellulosic ethanol production. Reactions were performed in biphasic media to increase reaction selectivity.

## 2. Results and Discussion

### 2.1. Preliminary Studies

The purpose of the preliminary studies was to optimize the reaction media and select the best catalytic metal for heterogeneous catalysts.

#### 2.1.1. Furfural Partitioning in Biphasic Reaction System

The reaction system was optimized in terms of the appropriate organic solvent and solvent:water ratio. Experiments were carried out using a 4.7 wt% furfural solution in water as feed and toluene or methyl isobutyl ketone (MIBK) as an organic solvent. The purpose was to compare furfural partitioning from water into these two solvents. Solvent ratios of 1:1, 1:2 and 1:3 were used based on the literature [17,27,28]. The results of partitioning experiments are shown in Figure 1, and, as expected,

the more organic solvent was added, the better furfural was extracted to the organic phase (Figure 1a). MIBK showed a better ability to extract furfural than toluene, as the furfural content in water was relatively higher in the toluene experiments than in the MIBK experiments. In the best case, when 1:3 water:MIBK was used as a solvent, 96% of furfural was extracted to the MIBK phase. Similarly, MIBK was reported to extract furfural better than toluene in the literature [27,29]. MIBK has a polar carbonyl group structure that may interact better with furfural, which is an aldehyde, compared to nonpolar toluene. The partitioning coefficient of MIBK has been reported to be 7 [29], while in our study it was 8 using a similar solvent ratio (1:1) and 8.5 when the solvent ratio was 1:3 (Figure 1b). For toluene, the partitioning coefficient has been reported to be 3 [29] but in our study it was significantly higher (6) with a 1:1 solvent ratio. Differences in reported and measured partitioning coefficients are likely due to different experimental setups. In the cited study, the partitioning coefficients were determined without any heating, using only shaking as an extraction technique. In our study, 5 min microwave heating (at 160 °C) was used, as the higher temperature corresponds to the reaction conditions in conversion. Based on the partitioning results, MIBK was considered most suitable for the furfural removal from water and it was used as an organic solvent in further experiments.

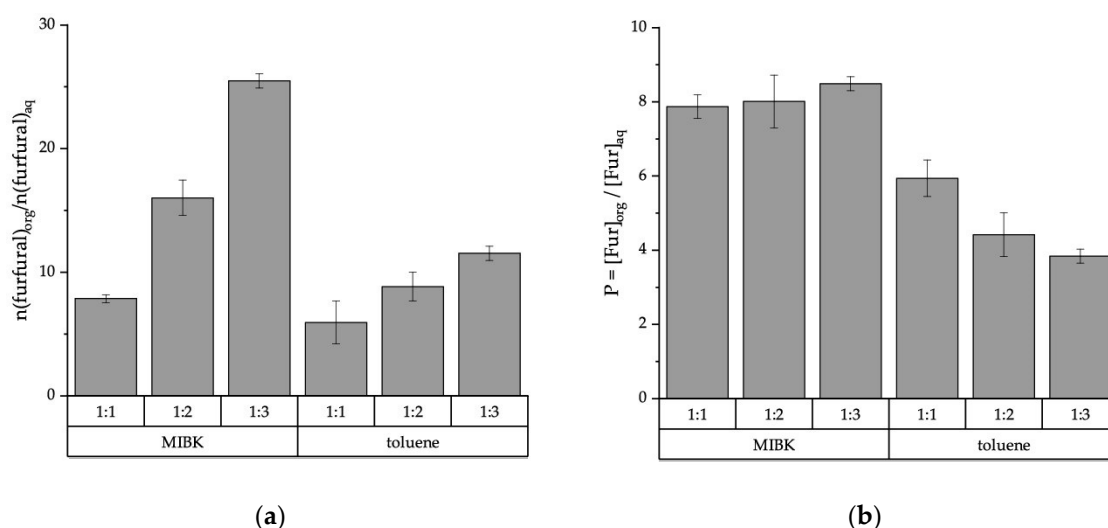


**Figure 1.** Furfural partitioning between water and methyl isobutyl ketone (MIBK) and water and toluene using different solvent ratios. (a) Partitioning calculated as the ratio of moles of furfural in the organic phase and in the water phase; (b) Partitioning calculated as the partitioning coefficient (based on concentrations).

### 2.1.2. Furfural Production Using Homogeneous Catalysts

After choosing the reaction media, homogeneous metal salts ( $\text{ZnCl}_2$ ,  $\text{AlCl}_3 \cdot 6\text{H}_2\text{O}$ ,  $\text{CrCl}_3 \cdot 6\text{H}_2\text{O}$ ,  $\text{SnCl}_2 \cdot 2\text{H}_2\text{O}$  and  $\text{FeCl}_3 \cdot 6\text{H}_2\text{O}$ ) were used as catalysts to determine the best metal for furfural production. Different metal salts have been studied in the literature but it was important to perform tests in our reaction system, using microwave heating and water/MIBK media. Reactions were performed at a temperature of 160 °C, a reaction time of 1.5 h and a catalyst amount of 0.05 mmol, based on the literature [10]. Almost full xylose conversion (98%–99%) was achieved using all catalysts other than zinc chloride, which yielded only 91% conversion (Figure 2, asterisks). In the furfural yields, there was variation between catalysts and the yields varied between 33% and 68% (Figure 2, bars). Chromium chloride and aluminum chloride produced the lowest furfural yields, although the xylose conversion was almost complete. Therefore, their selectivities (34% and 38%, respectively) were poorest among all catalysts (Figure 2, squares). Tin chloride and zinc chloride produced slightly higher furfural yields compared to chromium or aluminum and their selectivities were also higher (46% and 48%, respectively). However, the significantly highest furfural yield (68%) and selectivity (70%) were

achieved using iron chloride as a catalyst. Our result agrees with the literature, as many studies have shown that  $\text{FeCl}_3$  produces the highest furfural yield in water media compared to other metal halides [7,10]. The 68% furfural yield achieved in our study with  $\text{FeCl}_3$  catalyst is also comparable to that found in other studies. For example, Ershova et al. achieved a 60.3% furfural yield in water at 180 °C, while Zhang et al. reported a 77% furfural yield in gamma-valerolactone at 160 °C [10,30]. However, in most studies NaCl has been used as a phase modifier, and, because  $\text{Cl}^-$  has been shown to catalyze furfural formation, it is difficult to compare those results to our study without NaCl [31–34].

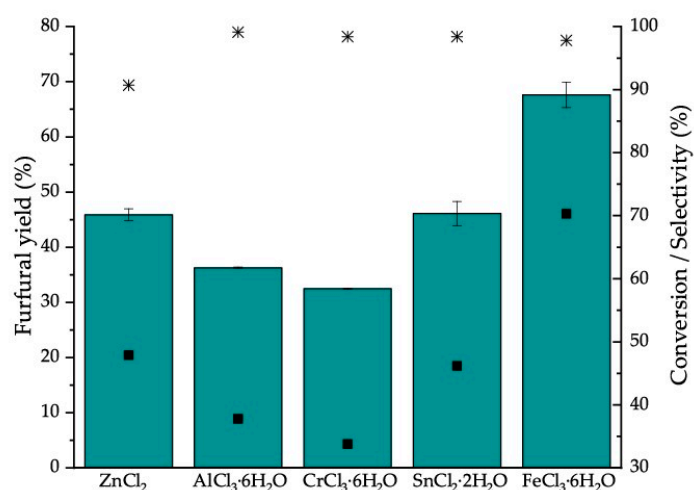


**Figure 2.** Furfural yield (bar), respective conversion (asterisk) and reaction selectivity (square) during xylose dehydration at 160 °C for 1.5 h using different metal chlorides (0.05 mmol) as catalysts.

## 2.2. Preparation and Characterization of Heterogeneous Catalysts

After the appropriate reaction media and catalytic metal were chosen, three different catalyst supports (ACz, ACz<sub>N</sub>, ACs) and five different catalysts (5FeNO<sub>3</sub>-ACz, 5Fe-ACz, 5Fe-ACz<sub>N</sub>, 5Fe-ACs and 10Fe-ACs) were prepared (Table 1). In the preparations, different activation methods, metal precursors, metal concentrations and additional treatments were used. ACz support was prepared applying common  $\text{ZnCl}_2$  chemical activation [35]. ACz-based catalysts 5FeNO<sub>3</sub>-ACz and 5Fe-ACz were prepared using 5 wt% of either  $\text{FeNO}_3$  or  $\text{FeCl}_3$  as an iron precursor, respectively. ACz<sub>N</sub> support was prepared using  $\text{HNO}_3$  treatment after  $\text{ZnCl}_2$  chemical activation and ACz<sub>N</sub>-based catalyst 5Fe-ACz<sub>N</sub> by further impregnation with  $\text{FeCl}_3$ . The third support type, ACs, was prepared using the physical activation method. Compared to chemical activation, physical activation is performed at a higher temperature but only using water steam as an activation agent [21,36]. ACs-based catalysts 5Fe-ACs and 10Fe-ACs were prepared using  $\text{FeCl}_3$  as a metal precursor and 5 or 10 wt% as the metal concentration.

**Table 1.** Key factors in the preparation of various supports and catalysts and the metal contents (wt%) of the prepared catalysts measured by inductively coupled plasma optical emission spectrometry (ICP-OES).

Sample	Activation Method	Other Treatment	Metal Precursor	Initial Fe (wt%)	Measured Metal (wt%)	
					Zn	Fe
ACs	Steam ( $\text{H}_2\text{O}$ )	-	-	-	0.01	0.06
5Fe-ACs	Steam ( $\text{H}_2\text{O}$ )	-	$\text{FeCl}_3$	5	-	4.0
10Fe-ACs	Steam ( $\text{H}_2\text{O}$ )	-	$\text{FeCl}_3$	10	-	9.2
ACz	$\text{ZnCl}_2$	-	-	-	8.2	0.08
5FeNO <sub>3</sub> -ACz	$\text{ZnCl}_2$	-	$\text{FeNO}_3$	5	4.6	5.0
5Fe-ACz	$\text{ZnCl}_2$	-	$\text{FeCl}_3$	5	3.8	4.5
ACz <sub>N</sub>	$\text{ZnCl}_2$	$\text{HNO}_3$	-	-	0.07	0.06
5Fe-ACz <sub>N</sub>	$\text{ZnCl}_2$	$\text{HNO}_3$	$\text{FeCl}_3$	5	0.08	5.5

The metal contents (according to inductively coupled plasma optical emission spectrometry (ICP-OES)) of all supports and catalysts are listed in Table 1. ACs support was analyzed most comprehensively since it was the least treated and therefore provided some indication about the metal content of the biomass-based lignin. According to the results, ACs contained minor amounts of metals, such as Ca (0.47 wt%) and Na (0.57 wt%) but its Fe content was very low (0.06 wt%) (Table S1). ACs-based iron-impregnated catalysts 5Fe-ACs and 10Fe-ACs contained 4.0 and 9.2 wt% iron, respectively. Based on these values, iron impregnation was considered successful, as the target amounts were 5 and 10 wt%. The other support, ACz, contained a significant amount of zinc (8.2 wt%), which originated from the chemical activation step in the preparation process. Zinc was also naturally present in ACz-supported 5Fe-ACz and 5FeNO<sub>3</sub>-ACz (3.8 and 4.6 wt%, respectively) but the amount decreased during the impregnation step. The iron contents for 5Fe-ACz and 5FeNO<sub>3</sub>-ACz were 4.5 and 5.0 wt%, respectively. Because of the remaining zinc, a third catalyst support ACz<sub>N</sub> was prepared similarly to ACz but afterwards it was treated with HNO<sub>3</sub> in order to remove remaining zinc. According to the ICP-OES results, this treatment did remove zinc because the remaining amount was only 0.07 wt%. Meanwhile, the iron content of 5Fe-ACz<sub>N</sub> was 5.5 wt%.

Additionally, the surface area (SA) according to Brunauer–Emmett–Teller (BET) theory, average pore diameter and pore volume distributions according to density functional theory (DFT) were determined for all supports and catalysts using N<sub>2</sub>-physisorption analysis (Table 2). As can be seen from the results, the surface area and pore volume of the chemically activated ACz and ACz<sub>N</sub> supports were higher (1470/1091 m<sup>2</sup>g<sup>−1</sup> and 0.72/0.49 cm<sup>3</sup>g<sup>−1</sup>) than for the ACs support prepared with steam activation (760 m<sup>2</sup>g<sup>−1</sup> and 0.47 cm<sup>3</sup>g<sup>−1</sup>) (entries 1, 4 and 7). Further, the total pore volume and the relative amount of micropores were higher in ACz and ACz<sub>N</sub> than in ACs. Treatment with HNO<sub>3</sub> after chemical activation decreased the support surface area, average pore diameter and total pore volume but the quantities were still greater than with steam activated ACs.

**Table 2.** N<sub>2</sub>-physisorption analysis from different activated carbon (AC) supports and catalysts.

Entry	Sample	BET		DFT		
		BET SA (m <sup>2</sup> /g)	Avg. Pore Diam. (nm)	Total Pore Volume (cm <sup>3</sup> /g)	Mesopores (cm <sup>3</sup> /g)	Micropores (cm <sup>3</sup> /g)
1	ACs	760	2.90	0.47	0.26	0.21
2	5Fe-ACs	455	3.44	0.34	0.23	0.11
3	10Fe-ACs	380	3.15	0.26	0.16	0.10
4	ACz	1470	2.29	0.72	0.31	0.41
5	5Fe-ACz	1000	2.28	0.48	0.19	0.29
6	5FeNO <sub>3</sub> -ACz	948	2.16	0.45 *	0.15	0.29
7	ACz <sub>N</sub>	1091	2.15	0.49	0.16	0.33
8	5Fe-ACz <sub>N</sub>	790	2.07	0.35	0.10	0.25

\* also contained macro-pores 0.01 cm<sup>3</sup>/g (3%).

The surface area and total pore volume of all catalysts decreased while the iron was impregnated on the carbon surface. This is reasonable, as metal is deposited on the surface and goes into the pores (Table 2). For ACs-based catalysts, the surface area decreased from 860 to 455 or 380 m<sup>2</sup>/g and total pore volume from 0.47 to 0.34 or 0.26 cm<sup>3</sup>/g, depending on how much metal was impregnated on the catalyst surface (entries 1–3). For ACz-based catalysts, the surface area decreased from 1470 to 1000 or 948 m<sup>2</sup>/g and the total pore volume from 0.72 to 0.48 or 0.45 cm<sup>3</sup>/g, depending on which iron precursor was used (entries 4–6). For ACz<sub>N</sub>-based catalysts, the surface area decreased from 1091 to 790 m<sup>2</sup>/g and the total pore volume decreased from 0.49 to 0.35 (entries 7–8).

Absolute volumes of the meso- and micropores decreased with all catalysts when iron was impregnated but there were differences in the final pore volume distributions between meso- and micropores, partly because of different initial pore volume distributions of the different supports.

For steam-activated ACs, the micropore volume decreased in 5Fe-ACs and 10Fe-ACs catalysts by 48%–52% compared to ACs. With mesopores, the decrease was smaller, only 12%–38%, meaning that the micropores were primarily filled in ACs when iron was impregnated. Because micropores were more filled with iron than mesopores, the average pore diameter also increased with ACs-based catalysts when compared to plain ACs. Comparing 5Fe-ACs and 10Fe-ACs, the difference in mesopore volume was notable, which meant that 5% iron addition did not affect the mesopores significantly while 10% iron addition filled the mesopores considerably. For chemically activated ACz and ACz<sub>N</sub>, the micropore volume decreased only 29% or 24%, respectively, while the volume of the mesopores was decreased 39%–52% for ACz and 38% for ACz<sub>N</sub>. Different precursors did not have a significant effect on surface area or pore volumes. Because the volume of the micropores decreased less than the volume of the mesopores, the relative amount of micropores was increased in chemically activated iron catalysts. In addition, the average pore diameter decreased compared to the supports.

Other surface properties, such as functional groups, acidity and detailed metal composition, were studied using X-ray photoelectron spectroscopy (XPS), the Boehm titration method and X-ray diffraction (XRD). These analyses were only conducted for ACs, 5Fe-ACs and 10Fe-ACs, which were determined to be the most promising ones in the conversion of xylose to furfural (see Section 2.3). XPS results show that plain ACs support already contains some oxygen functionalities (hydroxyl and carboxyl groups) on the surface but iron addition increases the oxygen–carbon ratio of the catalysts compared to ACs support (Table 3, Table S2). The increase is also dependent on how much iron is added, as the percentage of carbon atoms decreases from 96.8 to 93.6 or 86.3% and that of oxygen atoms increases from 2.9 to 4.1 or 9.5% when the amount of iron increased from 0.06 to 4.0 or to 9.2 wt%, respectively. In addition to C, O and Fe, Cl was detected from iron-impregnated catalysts. An increase of oxygen functionalities was detected from an O1s scan at 531.0eV and at 532.5eV (Table S2). The former can originate from carbonyl groups or metal oxides and the latter, for example, from hydroxyl groups or O-Fe bonds [37,38]. From the XPS Fe2p spectra, a peak at 711.3 eV was detected from both 5Fe-ACs and 10Fe-ACs catalysts, indicating the presence of oxidized iron, Fe<sub>2</sub>O<sub>3</sub> or FeOOH [37,39]. According to XRD, the iron was mostly present as oxides (Fe<sub>3</sub>O<sub>4</sub> and Fe<sub>2</sub>O<sub>3</sub>, Figure S1), so it is proposed that oxygen content was increased together with iron content as iron oxide. According to XRD, 10Fe-ACs contained mostly Fe<sub>2</sub>O<sub>3</sub> (hematite, 01-080-5405) and only small amounts of Fe<sub>3</sub>O<sub>4</sub> (magnetite, 04-015-9120). Conversely, 5Fe-ACs contained clearly more Fe<sub>3</sub>O<sub>4</sub> than Fe<sub>2</sub>O<sub>3</sub>. However, no iron chlorides were detected with XRD measurements.

**Table 3.** Surface analysis of prepared carbon support and catalysts according to X-ray photoelectron spectroscopy (XPS) and Boehm titration.

Sample	XPS <sup>a</sup>				Total Acidic Groups (mmol/g) <sup>b</sup>
	Total C-% from C1s	Total O-% from O1s	Total Fe-% from Fe2p	Total Cl-% from Cl2p	
ACs	96.8	3.0	nd	nd	0.07
5Fe-ACs	93.7	4.1	0.6	1.5	1.77
10Fe-ACs	86.2	9.6	2.4	1.6	1.95

<sup>a</sup> as atom-%, <sup>b</sup> by Boehm titration, nd = not detected.

According to Boehm titration, plain ACs contained a small amount of acidic oxygen functionalities (0.07 mmol/g, Table 3, Figure S2.). The amount of acidic oxygen groups increased when the metal was added to 1.77 or 1.95, depending on the metal amount. Acidic oxygen functionalities are probably formed during iron impregnation as a consequence of HCl formation from FeCl<sub>3</sub> hydration in water solution. Barroso-Bogeat et al. showed that metal ions markedly influence the pH of the impregnation solution and thereby the oxidizing power of this solution toward the activated carbon support [40]. Since XPS revealed the potential for the presence of iron hydroxides, it is possible that Brønsted acidity



of 5Fe-ACs and 10Fe-ACs is induced by iron hydroxides (e.g., FeOOH) [25,41]. Regardless of the specific nature of the acidic oxygen groups, they favor metal adsorption [42].

The morphology of the physically activated support (ACs) and catalysts (5Fe-ACs and 10Fe-ACs) was observed using a scanning electron microscope (SEM) and a scanning transmission electron microscope (STEM). SEM images clearly revealed particles on the carbon surface for 5Fe-ACs and 10Fe-ACs, while plain ACs did not contain any visible particles (Figure 3). The support and both catalysts showed a very porous structure in SEM as well as in STEM. Figure 4 (and Figure S3) shows chemical mapping of the elements C, O, Fe and Cl using energy-dispersive x-ray spectroscopy in scanning transmission electron microscopy (STEM-EDS). Comparing the distribution of Fe and O, it is clear that both elements appear at the same location, which indicates the presence of iron oxide. Therefore, the results obtained from XPS and XRD showing that the iron particles were oxides were confirmed. Mapping also showed that significant amount of residual chlorine was evenly distributed on the surface. Notable chlorine remains have been also detected in the literature when FeCl<sub>3</sub> has been used as a metal precursor [43].

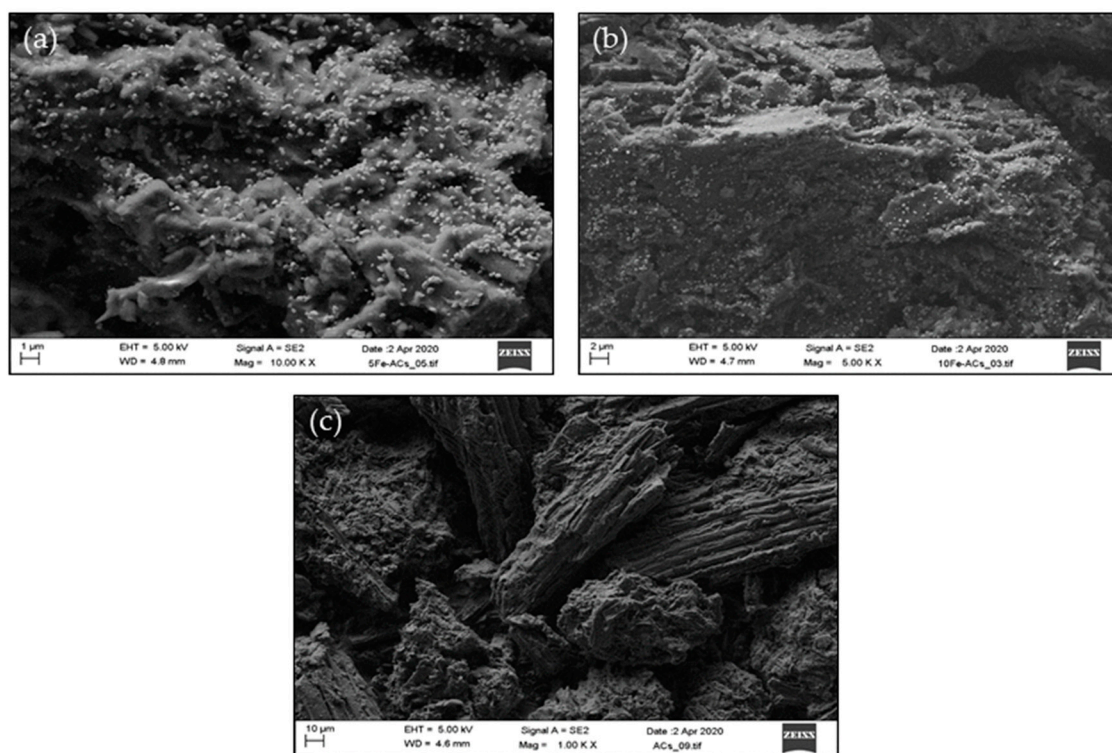


**Figure 3.** Scanning electron microscopy (SEM) images of 5Fe-ACs (a), 10Fe-ACs (b) and ACs (c). Iron particles are clearly visible in 5Fe-ACs and 10Fe-ACs while ACs shows a porous structure.

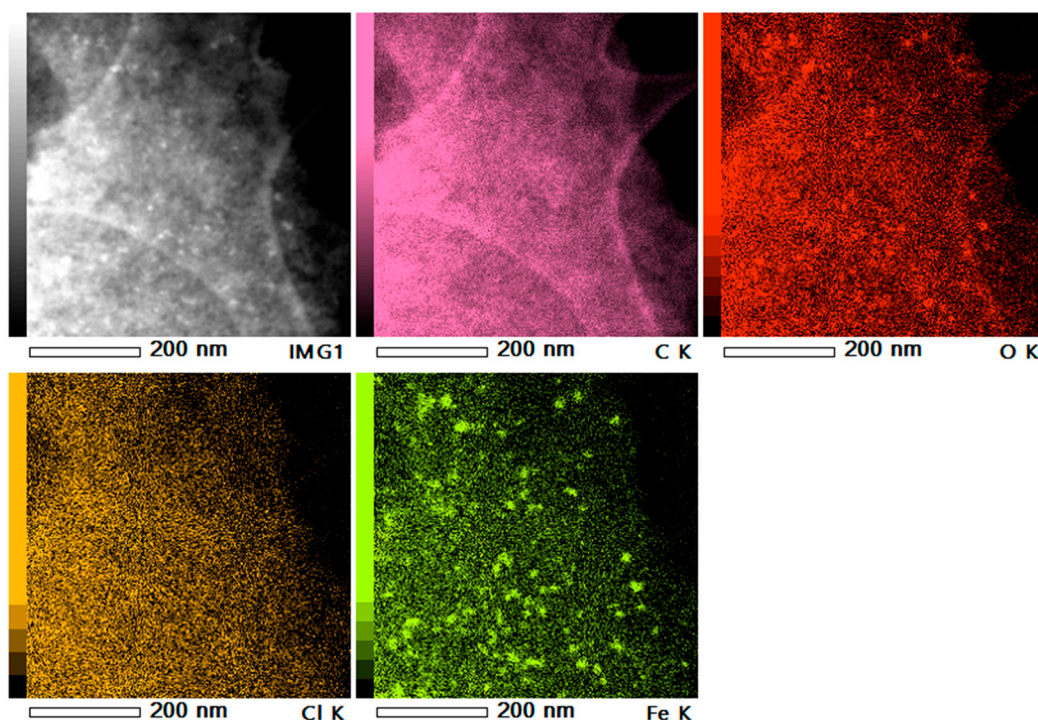


**Figure 4.** Chemical mapping of 5Fe-ACs using energy-dispersive x-ray spectroscopy in scanning transmission electron microscopy (STEM-EDS). The figure reveals that iron is most likely present as iron oxide on the carbon surface, as iron and oxygen appear in the same locations.

### 2.3. Furfural Production Using Heterogeneous Catalysts

Conversion studies were started with the control experiment without any support or catalyst (Table 4). This so-called autocatalysis was able to produce a 12% furfural yield and 18% xylose conversion at 160 °C in 1.5 h. Autocatalysis is based on high temperature and pressure, where the dissociation constant of water is increased [44]. In addition, formation of organic acids (e.g., formic and lactic acid) during the reaction might occur, which then further catalyzes the hydrolysis reaction [45]. However, a 160 °C reaction temperature and 1.5-h reaction time represent rather mild conditions and therefore only low conversion and yield were achieved. All supports and catalysts were able to produce higher furfural yields and conversions than the control experiment. First, chemically activated ( $\text{ZnCl}_2$ ) carbon support (ACz) was tested and it resulted in good conversion (82%, Table 4, entry 2). The furfural yield was also considerably high (28%). The high conversion is most likely connected to the high zinc content of ACz (Table 1), which originated from chemical activation. Iron was impregnated to the support using an  $\text{FeNO}_3$  precursor and  $\text{FeCl}_3$  precursor (Table 4, entries 3–4, respectively).  $\text{NO}_3$ -based salts are commonly favored as precursors since they leave no residue on the catalyst [46,47]. With a nitrate precursor, conversion increased further (from 82 to 91%) compared to ACz support but the yield decreased from 28 to 23% (Table 4, entries 2–3). Therefore, the reaction selectivity toward furfural also decreased (from 36 to 27%). With a chloride precursor, the yield increased (from 28 to 32%) compared to the ACz support and the reaction selectivity also increased (from 36 to 51%, Table 4, entries 2 and 4). Based on the higher furfural yield and reaction selectivity, the  $\text{FeCl}_3$  precursor was determined to be more suitable than  $\text{FeNO}_3$  and was used in further catalysts. Similar results were obtained by Chareonlimkun et al., who discovered that chloride-based precursors resulted in higher reactivity compared to nitrate-based precursors in  $\text{ZrO}$  and  $\text{TiO}$  catalysts [14]. As mentioned in Section 2.1.2, chloride ions have been shown to enhance furfural formation from xylose by favoring the 1,2-enediol formation before dehydration [34]. This is most probably reason why chlorine-based precursors increase furfural yield and reaction selectivity compared to nitrate-based precursors.



**Table 4.** Furfural yield, xylose conversion and reaction selectivity using various chemically activated catalysts at 160 °C with a 1.5-h reaction time.

Entry	Catalyst	Yield (%)	Conversion (%)	Selectivity (%)
1	-	12	18	12
2	ACz	28	82	36
3	5FeNO <sub>3</sub> -ACz	23	91	27
4	5Fe-ACz	32	66	51

Based on the results so far (Table 4), the 5Fe-ACz catalyst appeared to be the most promising catalyst. Therefore, it was used in conversion at different temperatures using various reaction times (Table 5, graphical presentation Figure S4). Temperature and reaction time are highly dependent on each other, so the time was increased at each temperature until the conversion reached 98%. At 160 °C, a 5 h reaction time was needed to achieve full xylose conversion (98%). In these conditions, the furfural yield was 48%. However, with a shorter 3-h reaction time, a similar furfural yield of 47% was achieved with lower conversion (89%). At a higher reaction temperature of 170 °C, the same 98% conversion was achieved in 2.5 h. However, the furfural yield was lower at this temperature with a 2.5 h reaction time (44%) compared to the yield at 160 °C but the highest 50% furfural yield was achieved with a shorter 2 h reaction time at 170 °C. At 180 °C, 99% conversion was obtained in 1.5 h but the furfural yield was low (39%). The highest reaction selectivities (55–56%) were achieved at 160 °C with 4 and 3 h reaction times and at 170 °C with a 2 h reaction time. At 180 °C, reaction selectivity was lowest because of the increasing amount of side reactions. Side reaction products were visible in chromatograms produced by high performance liquid chromatography (HPLC) (Figure S5).

**Table 5.** Effect of reaction temperature and time on furfural yield, xylose conversion and reaction selectivity using 5Fe-ACz as the catalyst. Y = furfural yield, C = xylose conversion, S = reaction selectivity.

Time	160 °C			170 °C			180 °C		
	Y (%)	C (%)	S (%)	Y (%)	C (%)	S (%)	Y (%)	C (%)	S (%)
1	25	50	54	36	82	46	38	97	41
1.5	32	66	51	44	93	49	39	99	41
2	38	79	51	50	96	55	-	-	-
2.5	38	85	48	44	98	48	-	-	-
3	47	89	55	-	-	-	-	-	-
4	47	95	56	-	-	-	-	-	-
5	48	98	54	-	-	-	-	-	-

Even though good furfural yields and reaction selectivities were achieved with 5Fe-ACz catalyst, there was some problems related to its stability. That is, all zinc already leached out of the catalyst at 160 °C in 3 h. In addition, a significant amount of iron (68–78% from initial, depending on reaction conditions) leached out of the catalyst. Therefore, more catalyst supports and catalysts were prepared and tested (Table 6). ACz<sub>N</sub> was chemically activated similarly to ACz but it was treated with HNO<sub>3</sub> after activation in order to remove remaining zinc. It produced a 14% furfural yield and 21% xylose conversion in 1.5 h at 160 °C (Table 6, entry 1), which is significantly less compared to ACz. However, the support was now zinc free (Table 1). When iron was impregnated on ACz<sub>N</sub>, the furfural yield increased from 14 to 22% and the conversion increased from 21 to 47% (Table 6, entries 1–2). The selectivity of 5Fe-ACz<sub>N</sub> was similar to that of 5Fe-ACz but the furfural yield and conversion were lower (Table 6, entry 2 and Table 4, entry 4). The third AC support, ACs, was physically steam activated with H<sub>2</sub>O instead of chemical activation. Its surface area was lower than that of ACz or ACz<sub>N</sub> because of the activation method but the conversion and furfural yields were comparable to ACz<sub>N</sub> (Table 6, entries 1 and 3). After iron impregnation to ACs, the furfural yield increased from 14 to 25% and the

conversion increased from 19 to 36%. The reaction selectivity with 5Fe-ACs was significantly higher than with any other iron catalyst: 72% compared to 27/50/51% (Tables 4 and 6).

**Table 6.** Furfural yield, xylose conversion and reaction selectivity using various catalysts at 160 °C with a 1.5-h reaction time.

Entry	Catalyst	Yield (%)	Conversion (%)	Selectivity (%)
1	ACz <sub>N</sub>	14	21	71
2	5Fe-ACz <sub>N</sub>	22	47	50
3	ACs	14	19	81
4	5Fe-ACs	25	36	72

To summarize the experiments so far, the chemical activation method with the AC support produced the best furfural yields before and after iron impregnation (Tables 4 and 6). However, catalyst characterization revealed that zinc chloride activation left some zinc remains in the catalyst support, which further affected its catalytic activity. Furthermore, all the zinc leached out of the catalyst during the first use and therefore the catalyst was suitable for a single use only. HNO<sub>3</sub>-treated chemically activated catalyst did not contain zinc remains but its catalytic activity in furfural production was comparable to that of physically activated ACs and its selectivity was lower than that of ACs. In addition, the chemical activation of ACz<sub>N</sub> demands significant amounts of ZnCl<sub>2</sub>, which is toxic to the environment. Therefore, the most reasonable carbon support for iron impregnation would be ACs, which does not require any chemicals other than water for preparation. As a precursor, FeCl<sub>3</sub> was more selective than FeNO<sub>3</sub>. The reaction temperature of 170 °C led to the highest furfural yield and thus it was chosen for further experiments.

Conversion studies were continued with ACs-based catalysts—5Fe-ACs and 10Fe-ACs. In addition, control experiments with plain ACs, without any catalyst and with a similar amount of homogeneous iron (as in 5Fe-ACs) were carried out. Reactions without any catalyst were able to produce at most a 37% furfural yield at 170 °C in 3.5 h (Figure 5, black squares). Conversion increased with time and reached 88% at highest. Conversion was notably higher at 170 °C than at the lower 160 °C reaction temperature and with a shorter 1.5-h reaction time (Table 4). The pH of the water phase also clearly changed to acidic during the reaction. In autocatalyzed reactions, furfural yields are strongly dependent on temperature and time but the highest furfural yields have been found around 50% [6]. Our 37% yield at 170 °C in 3.5 h is in good agreement with the study of Ershova et al., who achieved a 42% furfural yield at 180 °C in 3.75 h [10].

A plain activated carbon support (ACs) produced a similar furfural yield as water with all reaction times (Figure 5, red circles). Conversion was slightly higher, probably due to oxygen functionalities on the carbon surface (Table 3), until after 3 h reaction time it decreased slightly. Additionally, the selectivity was higher with ACs than with plain water. A 40% furfural yield and 77% conversion were the highest achieved with ACs in 3.5 h. When the activated carbon support was impregnated with iron, the furfural yield clearly increased. As expected, iron promoted furfural formation. Yields with both iron catalysts (5Fe-ACs and 10Fe-ACs) were similar with time (Figure 5, blue triangles up and green triangles down, respectively). The yields increased until a 3 h reaction time, after which they leveled off to 55–57% depending on the catalyst. The only exception was the 2.5 h reaction with 10Fe-ACs, in which the furfural yield did not increase when compared to the 2 h reaction. Conversion was similar with both the 5Fe-ACs and 10Fe-ACs catalysts and it increased with time from 59 to 96%. Conversion was clearly higher than with ACs or without a catalyst, which indicated that iron impregnation increased the catalysts' activities. Because the furfural yields and xylose conversions with 10Fe-ACs and 5Fe-ACs were so similar, it was concluded that 4 wt% iron was already enough to increase activated carbon catalyst activity and no benefit was obtained with a higher metal content. In fact, the reaction selectivity was lower with 10Fe-ACs than with 5Fe-ACs. The best reaction selectivity

(67%) was achieved with the 5Fe-ACs catalyst in 2 h but it did not decrease notably when the reaction time was increased to 3 h, which resulted in the highest furfural yield.

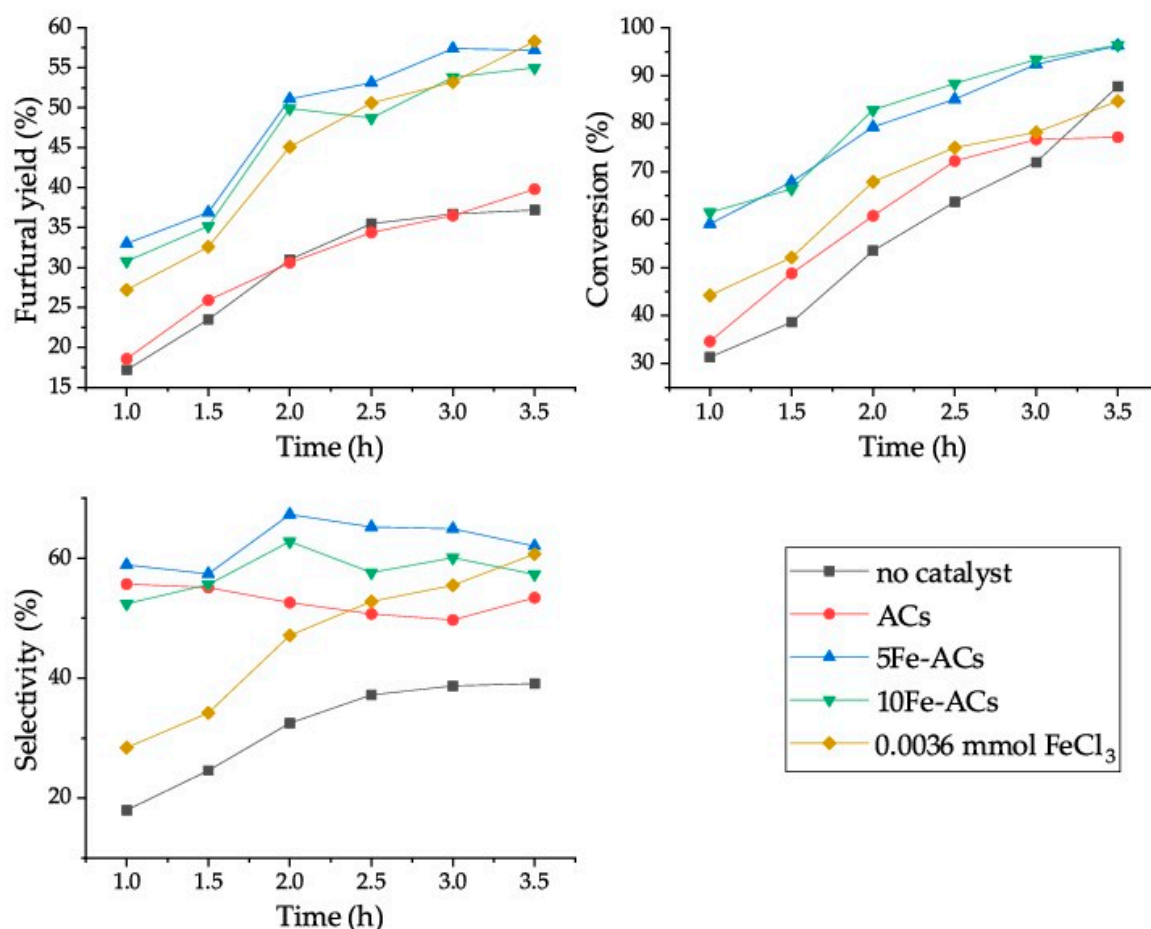


Figure 5. Furfural yield, xylose conversion and reaction selectivity using various catalysts at 170 °C.

Based on the previous results, 5Fe-ACs was the most promising catalyst studied. Therefore, it was compared to homogeneous  $\text{FeCl}_3 \cdot 6\text{H}_2\text{O}$  in similar conditions and using similar amounts of catalytic iron (Figure 5, brown rhombuses). A total of 0.0036 mmol of homogeneous  $\text{FeCl}_3 \cdot 6\text{H}_2\text{O}$  was able to produce a 27–58% furfural yield in 1–3.5 h. The yield was lower than with 5Fe-ACs until the reaction time reached 3.5 h. Even then, the increase in furfural yield was marginal compared to that with 5Fe-ACs, only one percentage unit. Conversion increased with time from 44 to 85% but was always clearly lower than with 5Fe-ACs. Reaction selectivity also increased with time from 28 to 61% but again it was always lower than with 5Fe-ACs. Better results with carbon-supported 5Fe-ACs than with homogeneous  $\text{FeCl}_3 \cdot 6\text{H}_2\text{O}$  demonstrated that activated carbon support is a promising option for furfural production. Based on catalyst characterization, iron was oxidized in a heterogeneous catalyst, which may have affected its catalytic activity positively compared to  $\text{FeCl}_3$ . Moreover, hydroxyl groups were detected on the surface of 5Fe-ACs, which increases the catalyst's Brønsted acid sites and therefore can increase furfural production.

The results with 5Fe-ACs (57% yield at 170 °C in 3 h) are comparable with studies using carbon-supported titanium catalysts—Mazzotta et al. reported a 51% furfural yield (180 °C, 30 min) in a biphasic MeTHF/water system, while Russo et al. achieved a 69% furfural yield (170 °C, 3.5 h) in toluene/water [22,23]. The results were higher than with sulfonated SBA- and MCM-supported metal oxide catalysts ( $\text{SBA-15/ZrO}_2\text{-Al}_2\text{O}_3/\text{SO}_4^{2-}$  and  $\text{MCM-41/ZrO}_2/\text{SO}_4^{2-}$ ), which resulted in 53 and 50% furfural yields, respectively, at 160 °C with a 4-h reaction time [15,16].

#### 2.4. Recycling Experiments

Catalyst recycling experiments were performed with 5Fe-ACs catalyst at 170 °C with a 3 h reaction time. After the reaction, the catalyst was filtered, washed with methanol and water, dried and then used again in the same conditions for three cycles. As a result, the furfural yield decreased from 48% to 30% after the first run and then remained constant (Figure 6). Conversion and reaction selectivity behaved similarly; conversion decreased from 76% to 53% and reaction selectivity from 66% to 59% after the first run and then they remained constant (Figure 6). The decrease in furfural yield, conversion and selectivity may be explained by iron leaching. Leaching was observed by measuring the iron content of the water phase after every reaction. After the first run, 66% of the initial iron amount was leached out but after second and third runs leaching was only 3% and 1%, respectively. It has been reported that hot acidic water promotes the solubility of some metal oxides and in particular the solubility of iron oxides is strongly influenced by the solution pH [48,49]. In our experiments, the pH changed from 6 to 2 during the reaction with 5Fe-ACs, so the reaction media was clearly acidic. Chang et al. were able to decrease iron leaching by post-treating the catalyst after impregnation, first with NaOH and then with HCl [43]. Post treatment was designated to convert iron to ferric hydroxide, which is poorly soluble in water. This treatment also decreased iron leaching at a low pH (pH = 2) to 21%, while the loss of iron during the post-treatment process was very minor (from 5.2 to 4.5 wt%). In future work, this must be taken into consideration.

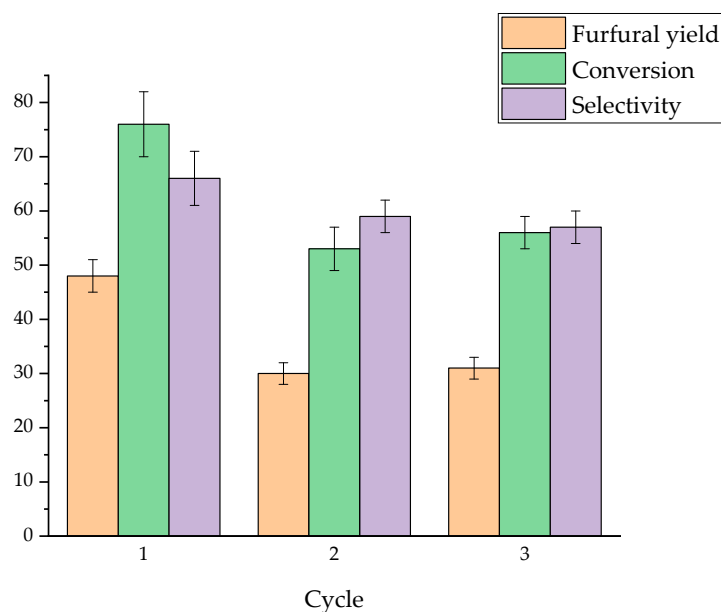


**Figure 6.** Furfural yield, xylose conversion and reaction selectivity in catalyst recycling experiments after 1–3 cycles.

The stability of the catalyst was also observed by monitoring changes at the catalyst surface with SEM and STEM. The images revealed that the iron content was decreased and leaching was more connected to larger iron particles (approx. 15–40 nm) than to small ones (approx. 5 nm) (see Figure S6). Small iron particles were present throughout the recycled catalysts, while large ones occurred only randomly. However, some large particles were also left on the catalyst surface after the third cycle, indicating that they were not all leached out. Leaching of large particles (or agglomerates of small particles) is reasonable since they are more vulnerable to leaching because they have poorer interaction with the support surface than smaller particles. In future work, it would be important to optimize the catalyst preparation to obtain less-agglomerated metal particles.

Based on catalyst weighing, the mass of the catalyst was increased from 5 to 6.7 mg in each cycle. This indicates that the catalyst was adsorbing some reaction products, such as humins. Humins



are black carbonaceous side-products generated either by the cross-polymerization of furfural by itself, between the just-formed furfural and free xylose present in solution or between furfural and intermediate products [50–52]. Solid humins can plug the pores of the catalyst surface, block the access of xylose to metal surface sites or totally encapsulate a metal particle [53]. It is also possible that this blocking of the catalytic sites on the porous structure of the catalyst caused the decrease in furfural yields. Indeed, pore blocking caused by carbon deposition is a common problem in heterogeneous porous catalysts; for example, with MCM-41-SO<sub>3</sub>H, the surface area and pore volume decreased by 50%–60% after the first run and the furfural yield decreased from 54% to 37% [54]. BET analysis of the used catalysts could not be performed because a very small amount of the catalysts was used in the reactions. In the SEM and STEM images, there was not any clear coating visible on the surface of the carbon, as in Reference [55] but some slight changes were observed in the SEM images (Figure S7). However, based on the figures, no differences were found between catalysts that were used one, two or three times.

### 3. Materials and Methods

#### 3.1. Materials

For catalyst preparation, hydrolysis lignin was obtained through a biomass hydrolysis process from Sekab Oy, Sweden. Other chemicals used in catalyst preparation, conversion reactions, partitioning experiments and analyses were used as received, without any purification. For high pressure liquid chromatography (HPLC) sample preparation, regenerated cellulose (RC) syringe filters (0.45 µm, 25 mm, Phenomenex) were used for the organic samples and polytetrafluoroethylene (PTFE) syringe filters (0.45 µm, 4 mm, Phenomenex) were used for the water samples.

#### 3.2. Furfural Partitioning in Biphasic Reactor System

Furfural partitioning experiments were carried out using a 4.7 wt% furfural solution in water as feed and toluene or MIBK as an organic solvent. The furfural solution and organic solvent were measured with alternative ratios (1:1, 1:2 and 1:3) into a microwave reactor tube with a magnetic stirring bar. The tube was closed, heated five minutes at 160 °C and cooled to room temperature. Samples from both layers were analyzed by HPLC to calculate the partitioning for furfural in different solvent systems.

#### 3.3. Catalyst Preparation and Characterization

Activated carbon (AC) supports were prepared from hydrolysis lignin, dried in oven at 105 °C and crushed to a particle size of <425 µm. Activation was performed using either a chemical or physical activation method. Chemical activation was done by impregnation of zinc chloride into the dried lignin using a 2:1 mass ratio of ZnCl<sub>2</sub>:biomass. ZnCl<sub>2</sub> dissolved into H<sub>2</sub>O was mixed with the biomass for 3 h at 85 °C and then dried in the oven at 105 °C until achieving a constant weight. The carbonization and activation of the dried ZnCl<sub>2</sub>-impregnated lignin was done in a stainless-steel tube in a tube furnace (Nabertherm RT200/13) (Nabertherm GmbH, Lilienthal, Germany) at 600 °C for 2 h using a heating ramp of 10 °C/min. During the thermal heating process, the reactor was flushed continuously with N<sub>2</sub> (flow 10 mL/min). Alternatively, carbonization followed by physical activation was performed in one-step process in a stainless-steel tube in a tube furnace using a heating ramp of 10 °C/min to 800 °C. At the target temperature, steam was added by feeding water at 0.5 mL/min into the reactor for 2 h. During the thermal heating process, the reactor was flushed continuously with N<sub>2</sub> (flow 10 mL/min). Both resulting activated carbons were washed with hot water, dried overnight at 105 °C, crushed and sieved to a fraction size of <100 µm. The supports were named AC<sub>z</sub> (AC zinc chloride-activated and water washed) and AC<sub>s</sub> (AC steam-activated and water washed). In addition, a support with chemical activation and HNO<sub>3</sub> treatment was prepared (AC<sub>zN</sub>). This was performed in a round bottom flask with a 10:1 mass ratio of 3 M HNO<sub>3</sub> per support and heated for 4 h at 85 °C. After

the acid treatment, the support was filtrated and washed with hot distilled water until neutral pH was obtained and finally it was dried in the oven at 105 °C.

In order to modify the carbon supports with iron, metal salts ( $\text{FeCl}_3 \cdot 6\text{H}_2\text{O}$  or  $\text{Fe}(\text{NO}_3)_3 \cdot 9\text{H}_2\text{O}$ ) were added by incipient wetness impregnation on the support, aiming that the targeted concentration of iron in the catalyst was 5 or 10 wt% of the total catalyst mass. The metal salts were dissolved in distilled water equal to the pore volume of the support and mixed with the support, matured for 5 h at room temperature and finally dried in an oven at 105 °C for 16 h. Finally, the catalysts were calcined at 400 °C for 2 h with a continuous flush of  $\text{N}_2$  (flow 10 mL/min). The iron-impregnated catalysts were named 5Fe-ACs, 10Fe-ACs, 5Fe<sub>NO3</sub>-ACz, 5Fe-ACz and 5Fe-ACz<sub>N</sub> according to the targeted iron concentration, type of support and type of iron precursor ( $\text{FeNO}_3$  if mentioned, otherwise  $\text{FeCl}_3$ ).

Specific SAs and pore size distributions were determined from the physisorption adsorption isotherms using nitrogen as the adsorbate. Determinations were performed with a Micromeritics ASAP 2020 instrument (Micromeritics Instrument, Norcross, GA, USA). Portions of each sample (100–200 mg) were degassed at low pressure (0.27 kPa) at a temperature of 140 °C for 3 h in order to remove adsorbed gas. Adsorption isotherms were obtained by immersing sample tubes in liquid nitrogen (−196 °C) to achieve constant temperature conditions. Gaseous nitrogen was added to the samples in small doses and the resulting isotherms were obtained. SAs were calculated from adsorption isotherms according to the BET (Brunauer–Emmett–Teller) method [56]. The percentual distribution of pore volumes (vol%) was calculated from the individual volumes of the micropores (pore diameter <2 nm), mesopores (pore diameter 2–50 nm) and macro-pores (diameter >50 nm) using the DFT (Density Functional Theory) model [57]. The instrumental setup enabled the measurement of micropores down to 1.5 nm in diameter, even if there might have been some contribution from smaller pores. The SAs were measured with a precision of ~5%.

The metal contents of the catalysts and supports were measured by ICP-OES using the 5110 VDV instrument (Agilent Technologies, Santa Clara, CA, USA). Zn, Fe, Ca, K, Mn, S, Na and Mg were measured from the ACs support; Zn and Fe contents were measured from ACz, 5Fe<sub>NO3</sub>-ACz, 5Fe-ACz, ACz<sub>N</sub> and 5Fe-ACz<sub>N</sub>; while only the Fe content was determined from 5Fe-ACs and 10Fe-ACs. For determination, samples of 0.1–0.2 g were first digested in a microwave oven (MARS, CEM Corporation) using the EPA 3051A method with 9 mL of  $\text{HNO}_3$  and 3 mL of  $\text{HCl}$  [58]. Subsequently, the solution was diluted to 50 mL with water and the former elements were analyzed with the ICP-OES.

XPS analyses were performed using the ESCALAB 250Xi XPS System (Thermo Fisher Scientific, Waltham, MA, USA). With a pass energy of 20 eV and a spot size of 900  $\mu\text{m}$ , the accuracy of the reported binding energies (BEs) was  $\pm 0.3$  eV. Fe, C, O and Cl were measured for all samples. The measurement data were analyzed using Avantage software. The monochromatic  $\text{AlK}\alpha$  radiation (1486.6 eV) was operated at 20 mA and 15 kV. Charge compensation of the BEs was performed by applying the  $\text{C1s}$  line at 284.8 eV as a reference.

XRD was used to study the phases of 5Fe-ACs and 10Fe-ACs utilizing PANalytical X'Pert Pro X-ray diffraction equipment (Malvern Panalytical, Almelo, Netherlands). The diffractograms were collected in the  $2\theta$  range of 5–90°, with a step size of 0.017° and a scan speed of 1.06°/min using monochromatic  $\text{CuK}\alpha 1$  radiation ( $\lambda = 1.5406 \text{ \AA}$ ) at 45 kV and 40 mA. The crystalline phases and structures were analyzed with HighScore Plus software and the peaks were identified using International Centre for Diffraction Data ICDD (PDF-4 + 2020).

The morphology of the catalyst particles was studied using SEM and STEM. A JEOL JEM-2200FS energy-filtered transmission electron microscope equipped with a scan generator (EFTEM/STEM) (JEOL Ltd., Tokyo, Japan) was used for STEM analysis. The catalyst samples were dispersed in pure ethanol and pretreated in an ultrasonic bath for several minutes to create a microemulsion. A small drop of the microemulsion was deposited on a copper grid pre-coated with carbon (Lacey/Carbon 200 Mesh Copper) and evaporated in air at room temperature. The accelerating voltage in the measurements was 200 kV, while the resolution of the STEM image was 0.2 nm. The metal particle sizes were estimated visually from the STEM high-angle annular dark field (HAADF) images. The SEM was performed

with a Zeiss Sigma Field emission scanning electron microscope (FESEM). In the sample preparation, a powder sample was placed on a conductive glue tape. The SEM images were taken at a voltage of 5 kV and a working distance around 5 mm.

Catalyst surface acidity was characterized by applying the Boehm titration method [59–63]. A total of 100 mg of catalyst was weighed and mixed with 50 mL 0.01 M NaOH. Samples were shaken (300 rpm) in sealed tubes for 72 h at room temperature and then filtered using a syringe and syringe filter (0.45  $\mu$ m, regenerated cellulose). Titration was carried out using a back-titration method by taking 10 mL of filtrate, mixing it with 20 mL of 0.01 M HCl and finally back-titrating with 0.01 M NaOH. Acidic groups were calculated using Equation (2), based on the theory that NaOH neutralizes all acidic oxygen groups (including phenols, lactonic groups and carboxylic acids) present on carbon. Nonconsumed base content was neutralized with acid and then nonconsumed acid was quantified through simple acid-base titration.

### 3.4. Furfural Production from Xylose

In a conversion reaction, 0.25 mmol (37.6 mg) of xylose and 0.0036/0.050 mmol of homogeneous metal salt ( $\text{AlCl}_3 \cdot 6\text{H}_2\text{O}$ ,  $\text{ZnCl}_2$ ,  $\text{CrCl}_3 \cdot 6\text{H}_2\text{O}$ ,  $\text{SnCl}_2 \cdot 2\text{H}_2\text{O}$  or  $\text{FeCl}_3 \cdot 6\text{H}_2\text{O}$ ) or 5 mg heterogeneous carbon-based catalyst were placed into a 5 mL reaction tube. A magnetic stirring bar, water (1 mL) and MIBK (3 mL) were added and the tube was sealed. The reaction was carried out in a Biotage Initiator microwave reactor (Biotage, Uppsala, Sweden) at 160/170/180 °C for 30 min to 3.5 h. After the reaction, approximate 1 mL samples from both layers were filtered with a syringe filter (an RC filter for the organic layer and a PTFE filter for the water layer) and then analyzed with HPLC.

### 3.5. Catalyst Recycling

Catalyst recycling experiments were carried out with 5Fe-ACs catalyst with a 3 h reaction time and a reaction temperature of 170 °C. After the reaction, liquid samples were taken normally for furfural and xylose analyses. In addition, metal leaching (Fe and Zn) was monitored by measuring the metal content of the water phase by AAS (see Section 3.6) and the catalyst was collected using a PALL Easy Pressure Syringe Filter Holder and hydrophilic polypropylene membrane (GHP). The catalyst was first washed with methanol (4 + 10 mL) and water (3\*10 mL) and then dried and weighed. Used catalysts were analyzed with SEM and TEM (see Section 3.3).

### 3.6. Analytical Methods for Conversion Studies

Two different HPLC analyses were used to detect furfural and xylose in the samples. In the analyses, calibrations were performed with commercial furfural or xylose. HPLC analysis for furfural was carried out using a Waters 2695 separation module fitted with an Atlantis T3 (3  $\mu$ m, 4.6  $\times$  150 mm) column and a Waters 996 photodiode array (PDA) detector (Waters Corp., Milford, MA, USA). A mixture of water (0.1% TFA) and methanol (0.1% TFA) (90:10) was used as the mobile phase, with a flow rate of 1 mL/min. The column temperature was kept constant at 30 °C and the UV detection for furfural was performed at 277 nm. HPLC analysis for xylose was carried out using a Shimadzu LC-20AT liquid chromatograph instrument fitted with an SIL-20A TH autosampler, RID-20A refractive index detector, SUGAR SH-G pre-column and Shodex SUGAR SH1821 column (8.0  $\times$  300 mm). Sulfuric acid (5 mM) was used as a mobile phase with a flow rate of 0.8 mL/min and the column temperature was kept constant at 60 °C.

Atomic absorption spectroscopy (AAS) was used to determine iron and zinc leaching from 5Fe-ACs and 5Fe-ACz catalysts. First, water phase samples of the reactions were diluted with water to a minimum 10 mL. Then, determinations were made using Varian AA240FS equipment (Varian Inc., Palo Alto, CA, USA), air-acetylene fuel, a Varian SpectrAA lamp (Cu/Mn/Zn/Fe) and flame emission wavelengths of 372.0 nm for Fe and 213.9 nm for Zn.

### 3.7. Equations

The partitioning coefficient (P) was calculated using the following formula:

$$P = [\text{furfural}]_{\text{org}}/[\text{furfural}]_{\text{aq}}, \quad (1)$$

where  $[\text{furfural}]_{\text{org}}$  is the concentration (g/l) of furfural in the organic layer and  $[\text{furfural}]_{\text{aq}}$  is the concentration of furfural in the water layer.

The total amount of acid sites according to Boehm titration was calculated as follows:

$$n_{\text{total acids}} = [(C_{\text{NaOH}} \cdot V_{\text{NaOH added}} - (C_{\text{HCl}} \cdot V_{\text{HCl added}} - C_{\text{NaOH}} \cdot V_{\text{NaOH titration}}) / \frac{1}{5}) - n_{\text{total acids in reference}}] / m, \quad (2)$$

where  $c$  (NaOH and HCl) are concentrations in mol/L,  $V$  (NaOH and HCl) are added volumes in mL,  $V$  (NaOH titration) is the volume of NaOH in mL needed to achieve equilibrium in titration,  $m$  is the mass of carbon weighed and  $n$  (total acids in reference) represents a blank solution without carbon. The factor  $\frac{1}{5}$  is due to the measurement of the 10 mL aliquots representing  $\frac{1}{5}$  of the reaction base.

The yield of furfural was calculated as follows:

$$Y_{\text{furfural}} (\%) = [c_{\text{furf meas org}} / c_{\text{furf max}}] \times 100\%, \quad (3)$$

where  $c_{\text{furf meas org}}$  is the measured furfural concentration in the organic phase of the sample and  $c_{\text{furf max}}$  is the theoretical maximum concentration of furfural in the sample.

The conversion of xylose was calculated as follows:

$$C_{\text{xylose}} (\%) = [n_{\text{xyl initial}} / n_{\text{xyl final}}] \times 100\%, \quad (4)$$

where  $n_{\text{xyl initial}}$  is the initial amount of xylose (in moles) fed to the reaction and  $n_{\text{xyl final}}$  is the amount of xylose left in the reaction mixture after the reaction.

The selectivity of the xylose to furfural conversion was calculated as follows:

$$S (\%) = [(c_{\text{furf meas total}} / c_{\text{furf max}}) / \text{conversion}] \times 100\%, \quad (5)$$

where  $c_{\text{furf meas total}}$  is the measured total furfural concentration in the organic and aqueous phases of the sample and  $c_{\text{furf max}}$  is the theoretical maximum concentration of furfural in the sample.

## 4. Conclusions

In this study, the conversion of xylose to furfural was studied using lignin-based activated carbon-supported iron oxide catalysts. Three different activated carbon supports and five different catalysts were prepared and studied in furfural production. Different activation methods, metal precursors and metal concentrations were used for the catalysts and different temperatures and reaction times were studied in the conversion reactions. Chemical activation resulted in a higher surface area and pore volume than physical activation but in conversion reactions, physically activated catalysts produced better reaction selectivity.  $\text{FeNO}_3$  precursor yielded higher xylose conversion than  $\text{FeCl}_3$  precursor but the furfural yield and selectivity were higher with  $\text{FeCl}_3$  precursor. The best results for xylose conversion to furfural were achieved with a 4 wt% iron-containing catalyst (5Fe-ACs), which produced a 57% yield, 92% conversion and 65% selectivity at 170 °C in 3 h. The results with a catalyst containing more iron (9.2 wt%) were lower (54% yield, 93% conversion and 60% selectivity) in similar conditions. The catalytic amount of Fe in 5Fe-ACs was only 3.6  $\mu\text{mol}$  and using this amount of homogeneous  $\text{FeCl}_3$  as a catalyst, reduced the furfural yield, xylose conversion and selectivity. Based on catalyst characterization, iron was in the form of iron oxide on the surface of the heterogeneous catalyst, which may have affected to its catalytic activity positively compared to  $\text{FeCl}_3$ . Moreover, hydroxyl groups were detected on the surface of 5Fe-ACs, which increases catalyst Brønsted acid



sites and therefore can increase furfural production. The recycling experiments revealed that part of the iron is easily leached out of the catalyst at a high temperature and in acidic conditions and the catalyst adsorbed some reactions products. These factors decreased the furfural yield and xylose conversion after the first round of recycling but then they remained constant. Although the activated carbon-supported iron oxide catalyst needs some improvements for better stability, it is a feasible alternative to homogeneous  $\text{FeCl}_3$ .

**Supplementary Materials:** The following are available online at <http://www.mdpi.com/2073-4344/10/8/821/s1>, Table S1: Metal analysis from ACs by ICP-OES, Table S2: XPS results of ACs, 5-Fe-ACs and 10Fe-ACs, Figure S1: XRD results of 5Fe-ACs and 10Fe-ACs, Figure S2: Boehm titration curves, Figure S3: EDS spectra of area shown in Figure 4, Figure S4: Graphical presentation of the results presented in Table 5, Figure S5: HPLC chromatogram of water (a) and organic (b) phase of reaction solution using 5Fe-ACz catalyst. Grams show increasing side product peak at 3.1 min and furfural shoulder at 8.5 min, when 180 °C was used as reaction temperature, Figure S6: STEM HAADF image of three times used 5Fe-ACs, which shows large agglomerated iron particles (diameter approx. 15–40 nm) as well as small single particles (diameter approx. 5 nm), Figure S7: SEM images of unused 5Fe-ACs (a,c) and used 5Fe-ACs (b,d) catalysts.

**Author Contributions:** Conceptualization, A.R.; methodology, A.R. and R.K.; formal analysis, A.R., R.K. and T.H.; investigation, A.R. and R.K.; data curation, A.R.; writing—original draft preparation, A.R.; writing—review and editing, K.L., R.K., J.K., T.H. and U.L.; visualization, A.R.; supervision, K.L., J.K. and U.L.; funding acquisition, A.R., U.L. and K.L. All authors have read and agreed to the published version of the manuscript.

**Funding:** This research was funded by Fortum Foundation, grant numbers 201800022 and 20190005, the EU/Interreg Botnia-Atlantica, grant number 20201508, the Foundation of Tauno Tönnig, grant number 20190154 and Nessling Foundation, grant number 201800070.

**Acknowledgments:** Sari Tuikkanen is acknowledged for completing part of HPLC measurements and Riina Hemmilä for AAS-measurements.

**Conflicts of Interest:** The authors declare no conflict of interest.

## References

1. Werpy, T.; Petersen, G. *Top Value Added Chemicals from Biomass: Volume I—Results of Screening for Potential Candidates from Sugars and Synthesis Gas*; U.S. Department of Energy: Washington, DC, USA, 2004. [CrossRef]
2. Kottke, R.H. Furan derivatives. In *Encyclopedia of Chemical Technology*; Othmer, K., Ed.; John Wiley & Sons, Inc.: New York, NY, USA, 2000; Volume 12, pp. 259–286. [CrossRef]
3. Eseyin, A.E.; Steele, P.H. An overview of the applications of furfural and its derivatives. *Int. J. Adv. Chem.* **2015**, *3*, 42–47. [CrossRef]
4. Win, D. Furfural—Gold from Garbage. *Au J. Technol.* **2005**, *8*, 185–190.
5. Zeitsch, K. *The Chemistry and Technology of Furfural and its Many By-Products*; Elsevier: Amsterdam, The Netherlands, 2000; pp. 36–74.
6. Dashtban, M.; Gilbert, A.; Fatehi, P. Production of furfural: Overview and challenges. *J. Sci. Technol. For. Prod. Process* **2012**, *2*, 44–53.
7. Yemis, O.; Mazza, G. Catalytic Performances of Various Solid Catalysts and Metal Halides for Microwave-Assisted Hydrothermal Conversion of Xylose, Xylan, and Straw to Furfural. *Waste Biomass Valori.* **2019**, *10*, 1343–1353. [CrossRef]
8. Le Guenic, S.; Delbecq, F.; Ceballos, C.; Len, C. Microwave-assisted dehydration of D-xylose into furfural by diluted inexpensive inorganic salts solution in a biphasic system. *J. Mol. Catal. A Chem.* **2015**, *410*, 1–7. [CrossRef]
9. Liu, C.; Wyman, C.E. The enhancement of xylose monomer and xylotriose degradation by inorganic salts in aqueous solutions at 180 °C. *Carbohydr. Res.* **2006**, *341*, 2550–2556. [CrossRef]
10. Ershova, O.; Nieminen, K.; Sixta, H. The Role of Various Chlorides on Xylose Conversion to Furfural: Experiments and Kinetic Modeling. *Chem. Cat. Chem.* **2017**, *9*, 3031–3040. [CrossRef]
11. Romo, J.E.; Bollar, N.V.; Zimmermann, C.J.; Wettstein, S.G. Conversion of Sugars and Biomass to Furans Using Heterogeneous Catalysts in Biphasic Solvent Systems. *Chem. Cat. Chem.* **2018**, *10*, 4819–4830. [CrossRef]

12. Da Costa Lopez, A.M.; Morais, A.R.C.; Lukasik, R.M.; Fang, Z.; Smith, R.L., Jr.; Qi, X. Sustainable Catalytic Strategies for C5-Sugars and Biomass Hemicellulose Conversion Towards Furfural Production. In *Production of Platform Chemicals from Sustainable Resources*; Springer Nature: Singapore, 2017; Volume 7, pp. 45–80. [\[CrossRef\]](#)
13. Zhang, J.; Lin, L.; Liu, S. Efficient Production of Furan Derivatives from a Sugar Mixture by Catalytic. *Process. Energ. Fuel* **2012**, *26*, 4560–4567. [\[CrossRef\]](#)
14. Chareonlimkun, A.; Champreda, V.; Shotipruk, A.; Laosiripojana, N. Reactions of C5 and C6-sugars, cellulose, and lignocellulose under hot compressed water (HCW) in the presence of heterogeneous acid catalysts. *Fuel* **2010**, *89*, 2873–2880. [\[CrossRef\]](#)
15. Shi, X.; Wu, Y.; Li, P.; Yi, H.; Yang, M.; Wang, G. Catalytic conversion of xylose to furfural over the solid acid SO<sub>4</sub><sup>2-</sup>/ZrO<sub>2</sub>-Al<sub>2</sub>O<sub>3</sub>/SBA-15 catalysts. *Carbohydr. Res.* **2011**, *346*, 480–487. [\[CrossRef\]](#)
16. Dias, A.S.; Pillinger, M.; Valente, A.A. Mesoporous silica-supported 12-tungstophosphoric acid catalysts for the liquid phase dehydration of d-xylose. *Micropor. Mesopor. Mater.* **2006**, *94*, 214–225. [\[CrossRef\]](#)
17. Weingarten, R.; Cho, J.; Conner, W.C., Jr.; Huber, G.W. Kinetics of furfural production by dehydration of xylose in a biphasic reactor with microwave heating. *Green Chem.* **2010**, *12*, 1423–1429. [\[CrossRef\]](#)
18. Choudhary, V.; Pinar, A.B.; Sandler, S.I.; Vlachos, D.G.; Lobo, R.F. Xylose Isomerization to Xylulose and its Dehydration to Furfural in Aqueous Media. *ACS Catal.* **2011**, *1*, 1724–1728. [\[CrossRef\]](#)
19. Choudhary, V.; Sandler, S.I.; Vlachos, D.G. Conversion of Xylose to Furfural Using Lewis and Brønsted Acid Catalysts in Aqueous Media. *ACS Catal.* **2012**, *2*, 2022–2028. [\[CrossRef\]](#)
20. Rodríguez-Reinoso, F. The role of carbon materials in heterogeneous catalysis. *Carbon* **1998**, *36*, 159–175. [\[CrossRef\]](#)
21. Rodríguez-Reinoso, F.; Molina-Sabio, M. Activated carbons from lignocellulosic materials by chemical and/or physical activation: An overview. *Carbon* **1992**, *30*, 1111–1118. [\[CrossRef\]](#)
22. Mazzotta, M.G.; Gupta, D.; Saha, B.; Patra, A.K.; Bhaumik, A.; Abu-Omar, M.M. Efficient Solid Acid Catalyst Containing Lewis and Brønsted Acid Sites for the Production of Furfurals. *ChemSusChem* **2014**, *7*, 2342–2350. [\[CrossRef\]](#)
23. Russo, P.A.; Lima, S.; Rebutini, V.; Pillinger, M.; Willinger, M.; Pinna, N.; Valente, A.A. Microwave-assisted coating of carbon nanostructures with titanium dioxide for the catalytic dehydration of d-xylose into furfural. *RSC Adv.* **2013**, *3*, 2595–2603. [\[CrossRef\]](#)
24. Barroso-Bogeat, A.; Alexandre-Franco, M.; Fernández-González, C.; Gómez-Serrano, V. Preparation of activated carbon-metal oxide hybrid catalysts: Textural characterization. *Fuel Process. Technol.* **2014**, *126*, 95–103. [\[CrossRef\]](#)
25. Barroso-Bogeat, A.; Alexandre-Franco, M.; Fernández-González, C.; Gómez-Serrano, V. Preparation and Microstructural Characterization of Activated Carbon–Metal Oxide Hybrid Catalysts: New Insights into Reaction Paths. *J. Mater. Sci. Technol.* **2015**, *31*, 806–814. [\[CrossRef\]](#)
26. Barroso-Bogeat, A.; Alexandre-Franco, M.; Fernández-González, C.; Macías-García, A.; Gómez-Serrano, V. Preparation of Activated Carbon-SnO<sub>2</sub>, TiO<sub>2</sub>, and WO<sub>3</sub> Catalysts. Study by FT-IR Spectroscopy. *Ind. Eng. Chem. Res.* **2016**, *55*, 5200–5206. [\[CrossRef\]](#)
27. Mittal, A.; Black, S.K.; Vinzant, T.B.; O'Brien, M.; Tucker, M.P.; Johnson, D.K. Production of Furfural from Process-Relevant Biomass-Derived Pentoses in a Biphasic Reaction System. *ACS Sustain. Chem. Eng.* **2017**, *5*, 5694–5701. [\[CrossRef\]](#)
28. Moreau, C.; Durand, R.; Peyron, D.; Duhamet, J.; Rivalier, P. Selective preparation of furfural from xylose over microporous solid acid catalysts. *Ind. Crops Prod.* **1998**, *7*, 95–99. [\[CrossRef\]](#)
29. Brouwer, T.; Blahusiak, M.; Babic, K.; Schuur, B. Reactive extraction and recovery of levulinic acid, formic acid and furfural from aqueous solutions containing sulphuric acid. *Sep. Purif. Technol.* **2017**, *185*, 186–195. [\[CrossRef\]](#)
30. Zhang, L.; Yu, H.; Wang, P.; Li, Y. Production of furfural from xylose, xylan and corncob in gamma-valerolactone using FeCl<sub>3</sub>·6H<sub>2</sub>O as catalyst. *Bioresour. Technol.* **2014**, *151*, 355–360. [\[CrossRef\]](#)
31. Vom Stein, T.; Grande, P.M.; Leitner, W.; Dominguez de Maria, P. Iron-Catalyzed Furfural Production in Biobased Biphasic Systems: From Pure Sugars to Direct Use of Crude Xylose Effluents as Feedstock. *ChemSusChem* **2011**, *4*, 1592–1594. [\[CrossRef\]](#)
32. Zhang, Y.; Chen, M.; Wang, J.; Hu, Q. Furfural production from dehydration of xylose catalyzed by chromium chloride in biphasic system. *Chem. Eng.* **2014**, *3*, 54–58. [\[CrossRef\]](#)

33. Yang, Y.; Hu, C.; Abu-Omar, M.M. Conversion of carbohydrates and lignocellulosic biomass into 5-hydroxymethylfurfural using  $\text{AlCl}_3 \cdot 6\text{H}_2\text{O}$  catalyst in a biphasic solvent system. *Green Chem.* **2012**, *14*, 509–513. [\[CrossRef\]](#)
34. Marcotullio, G.; Jong, W.D. Chloride ions enhance furfural formation from D-xylose in dilute aqueous acidic solutions. *Green Chem.* **2010**, *12*, 1739–1746. [\[CrossRef\]](#)
35. Varila, T.; Bergna, D.; Lahti, R.; Romar, H.; Hu, T.; Lassi, U. Activated carbon production from peat using  $\text{ZnCl}_2$ : Characterization and applications. *Bioresources* **2017**, *12*, 8078–8092. [\[CrossRef\]](#)
36. Lahti, R.; Bergna, D.; Romar, H.; Tuuttila, T.; Hu, T.; Lassi, U. Physico-chemical properties and use of waste biomass-derived activated carbons. *Chem. Eng. Trans.* **2017**, *57*. [\[CrossRef\]](#)
37. Brion, D. Etude par spectroscopie de photoelectrons de la degradation superficielle de  $\text{FeS}_2$ ,  $\text{CuFeS}_2$ ,  $\text{ZnS}$  et  $\text{PbS}$  a l'air et dans l'eau. *Appl. Surf. Sci.* **1980**, *5*, 133–152. [\[CrossRef\]](#)
38. Moulder, J.F.; Stickle, W.F.; Sobol, P.E.; Bomben, K.D. *Handbook of X-ray Photoelectron Spectroscopy*; Perkin-Elmer Corporation: Eden Prairie, MN, USA, 1992; p. 45.
39. Li, J.; Liu, J.; Zhou, H.; Fu, Y. Catalytic Transfer Hydrogenation of Furfural to Furfuryl Alcohol over Nitrogen-Doped Carbon-Supported Iron Catalysts. *ChemSusChem* **2016**, *9*, 1339–1347. [\[CrossRef\]](#)
40. Barroso-Bogeat, A.; Alexandre-Franco, M.; Fernández-González, C.; Gómez-Serrano, V. Activated carbon surface chemistry: Changes upon impregnation with  $\text{Al(III)}$ ,  $\text{Fe(III)}$  and  $\text{Zn(II)}$ -metal oxide catalyst precursors from  $\text{NO}_3^-$  aqueous solutions. *Arab. J. Chem.* **2019**, *12*, 3963–3976. [\[CrossRef\]](#)
41. Xiong, Y.; Tong, Q.; Shan, W.; Xing, Z.; Wang, Y.; Wen, S.; Lou, Z. Arsenic transformation and adsorption by iron hydroxide/manganese dioxide doped straw activated carbon. *Appl. Surf. Sci.* **2017**, *416*, 618–627. [\[CrossRef\]](#)
42. Pakula, M.; Biniak, S.; Świątkowski, A. Chemical and Electrochemical Studies of Interactions between Iron(III) Ions and an Activated Carbon Surface. *Langmuir* **1998**, *14*, 3082–3089. [\[CrossRef\]](#)
43. Chang, Q.; Lin, W.; Ying, W. Preparation of iron-impregnated granular activated carbon for arsenic removal from drinking water. *J. Hazard. Mater.* **2010**, *184*, 515–522. [\[CrossRef\]](#)
44. Dallinger, D.; Kappe, C.O. Microwave-Assisted Synthesis in Water as Solvent. *Chem. Rev.* **2007**, *107*, 2563–2591. [\[CrossRef\]](#)
45. Antal, M.J.; Leesomboon, T.; Mok, W.S.; Richards, G.N. Mechanism of formation of 2-furaldehyde from d-xylose. *Carbohydr. Res.* **1991**, *217*, 71–85. [\[CrossRef\]](#)
46. Hutchings, G.J.; Védrine, J.C. Heterogeneous Catalyst Preparation. In *Basic Principles in Applied Catalysis*; Baerns, M., Ed.; Springer: Berlin, Germany, 2004; Volume 75, pp. 215–257. [\[CrossRef\]](#)
47. Jüntgen, H. Activated carbon as catalyst support: A review of new research results. *Fuel* **1986**, *65*, 1436–1446. [\[CrossRef\]](#)
48. Matatov-Meytal, Y.I.; Sheintuch, M. Catalytic Abatement of Water Pollutants. *Ind. Eng. Chem. Res.* **1998**, *37*, 309–326. [\[CrossRef\]](#)
49. Kraemer, S.M. Iron oxide dissolution and solubility in the presence of siderophores. *Aquat. Sci.* **2004**, *66*, 3–18. [\[CrossRef\]](#)
50. Cheng, B.; Wang, X.; Lin, Q.; Zhang, X.; Meng, L.; Sun, R.; Xin, F.; Ren, J. New Understandings of the Relationship and Initial Formation Mechanism for Pseudo-lignin, Humins, and Acid-Induced Hydrothermal Carbon. *J. Agric. Food Chem.* **2018**, *66*, 11981–11989. [\[CrossRef\]](#) [\[PubMed\]](#)
51. Van Zandvoort, I.; Wang, Y.; Rasrendra, C.B.; van Eck, E.R.H.; Bruijninx, P.C.A.; Heeres, H.J.; Weckhuysen, B.M. Formation, Molecular Structure, and Morphology of Humins in Biomass Conversion: Influence of Feedstock and Processing Conditions. *ChemSusChem* **2013**, *6*, 1745–1758. [\[CrossRef\]](#) [\[PubMed\]](#)
52. Sumerskii, I.V.; Krutov, S.M.; Zarubin, M.Y. Humine-like substances formed under the conditions of industrial hydrolysis of wood. *Russ. J. Appl. Chem.* **2010**, *83*, 320–327. [\[CrossRef\]](#)
53. Bartholomew, C.H. Mechanisms of catalyst deactivation. *Appl. Catal. A Gen.* **2001**, *212*, 17–60. [\[CrossRef\]](#)
54. Dias, A.S.; Pillinger, M.; Valente, A.A. Dehydration of xylose into furfural over micro-mesoporous sulfonic acid catalysts. *J. Catal.* **2005**, *229*, 414–423. [\[CrossRef\]](#)
55. Jeong, G.H.; Kim, E.G.; Kim, S.B.; Park, E.D.; Kim, S.W. Fabrication of sulfonic acid modified mesoporous silica shells and their catalytic performance with dehydration reaction of d-xylose into furfural. *Micropor. Mesopor. Mater.* **2011**, *144*, 134–139. [\[CrossRef\]](#)
56. Brunauer, S.; Emmett, P.H.; Teller, E. Adsorption of Gases in Multimolecular Layers. *J. Am. Chem. Soc.* **1938**, *60*, 309–319. [\[CrossRef\]](#)

57. Seaton, N.A.; Walton, J.P.R.B.; Quirke, N. A new analysis method for the determination of the pore size distribution of porous carbons from nitrogen adsorption measurements. *Carbon* **1989**, *27*, 853–861. [[CrossRef](#)]
58. U.S. EPA. *Method 3051A (SW-846): Microwave Assisted Acid Digestion of Sediments, Sludges, and Oils*; U.S. EPA: Washington, DC, USA, 2007.
59. Boehm, H.P. Chemical Identification of Surface Groups. In *Advances in Catalysis*; Eley, D.D., Pines, H., Weisz, P.B., Eds.; Elsevier Academic Press: San Diego, CA, USA, 1966; Volume 16, pp. 179–274. [[CrossRef](#)]
60. Boehm, H.P. Some aspects of the surface chemistry of carbon blacks and other carbons. *Carbon* **1994**, *32*, 759–769. [[CrossRef](#)]
61. Schönherr, J.; Buchheim, J.R.; Scholz, P.; Adelhelm, P. Boehm titration revisited (part i): Practical aspects for achieving a high precision in quantifying oxygen-containing surface groups on carbon materials. *Carbon* **2018**, *4*, 21. [[CrossRef](#)]
62. Goertzen, S.L.; Theriault, K.D.; Oickle, A.M.; Tarasuk, A.C.; Andreas, H.A. Standardization of the Boehm titration. Part, I. CO<sub>2</sub> expulsion and endpoint determination. *Carbon* **2010**, *48*, 1252. [[CrossRef](#)]
63. Oickle, A.M.; Goertzen, S.L.; Hopper, K.R.; Abdalla, Y.O.; Andreas, H.A. Standardization of the Boehm titration: Part II. Method of agitation, effect of filtering and dilute titrant. *Carbon* **2010**, *48*, 3313–3322. [[CrossRef](#)]



© 2020 by the authors. Licensee MDPI, Basel, Switzerland. This article is an open access article distributed under the terms and conditions of the Creative Commons Attribution (CC BY) license (<http://creativecommons.org/licenses/by/4.0/>).